International Journal of Fatigue 105 (2017) 7–15

Contents lists available at ScienceDirect

International Journal of Fatigue

journal homepage: www.elsevier.com/locate/ijfatigue

Pre-notched and corroded low cycle fatigue behaviour of a nickel based alloy for disc rotor applications

M. Dowd [a,*], K.M. Perkins [b], D.J. Child [c]

[a] Institute of Structural Materials, Swansea University, Bay Campus, Swansea SA1 8EN, UK
[b] College of Engineering, Swansea University, Bay Campus, Swansea SA1 8EN, UK
[c] Rolls-Royce plc., P.O. Box 31, Derby DE24 8BJ, UK

ARTICLE INFO

Article history:
Received 9 May 2017
Received in revised form 1 August 2017
Accepted 11 August 2017
Available online 16 August 2017

Keywords:
Corrosion
Corrosion fatigue
Environmental assisted fatigue
Pitting corrosion
Superalloys

ABSTRACT

Currently there is doubt surrounding the suitability of chemically-induced stress independent pre-conditioning of specimens to simulate turbine corrosion prior to fatigue testing. The thick oxide scales developed using such techniques can lead to net section loss and typically a lack of grain boundary sulphide attack seen in components that experience stress. An alternative approach to a corrosion-fatigue test scenario is suggested by micro-notching fatigue specimens prior to low salt flux corrosion to form grain boundary sulphide particles within channel-like features akin to stress assisted morphologies. On fatigue testing, a trend was identified where a change of mechanism was observed. The grain boundary oxide likely formed in the wake of freshly precipitated sulphide particles fractures around segments of grains leading to a metal loss that contributes to a significant reduction in fatigue properties.

1. Introduction

As turbine entry temperatures are pushed higher to improve gas turbine efficiency, engine components are forced to accommodate increasingly higher stresses and temperatures. This places significant demands on the high strength nickel alloys used for critical parts; failure of these parts would threaten the safety of an aircraft and its passengers. In light of this, engines are routinely inspected for various forms of damage including handling, foreign object damage and environmental attack. Discs spending increased time at temperature have resulted in instances of corrosion damage detected on components within the declared life. As the turbine disc is a safety critical component, assessment of any surface damage is advantageous to understand the impact on remnant component life. Fig. 1 provides an example of the damage, where a roughly 'V' shaped region of grain loss resides at the surface. In addition, intergranular sulphide particles can be seen penetrating into the alloy. Recent corrosion-fatigue studies on salted specimens [1,2] have shown that a corrosive environment in conjunction with cyclic stress can give rise to similar pit shaped notch features that, depending on salt loading and stress level, reduces fatigue life in comparison to unsalted specimens tested in air.

Historically, the mechanisms of sodium sulphate (Na_2SO_4)-induced hot corrosion in Ni-base superalloys have been categorised as either type-I or type-II hot corrosion depending on the temperature of the system and is closely related to the melting point of the salt contaminant [3]. Type-I hot corrosion is generally observed above 900 °C and is characterised by discrete sulphide particles below a protective chromium oxide. In type-I hot corrosion, the mechanism proceeds as the molten Na_2SO_4 salt deposit causes the separation of alloy from the gas phase and due to low oxygen solubility in Na_2SO_4 [4], an O_2 gradient is established across the deposit. This gradient results in an increase in sulphur activity at the alloy surface, such that sulphur and oxygen is removed from the deposit by the alloy to form sulphides and oxides [5]. Type-II hot corrosion is observed in the temperature region of 650–800 °C and is characterised by a continuous sulphide layer below a dual oxide layer of Ni and Co on top of a mixed Cr, Ti and Al oxide. In type-II hot corrosion, given that Na_2SO_4 melts at 884 °C, the deposit would remain solid at the alloy surface. Hence, in order to propagate the mechanism, liquid formation of the deposit is achieved via the reaction of the SO_3 present in a typical turbine gas stream with transient metal oxides that form at the alloy surface during the early stages of oxidation. This reaction forms metal sulphate (MSO_4), which can dissolve into the Na_2SO_4 deposit to form a eutectic MSO_4-Na_2SO_4 melt [6]. The liquid melt separates the alloy from the gas phase and as the solubility of SO_3 across the deposit is high [4], decreases the oxygen activity of the deposit

* Corresponding author.
E-mail address: m.dowd@swansea.ac.uk (M. Dowd).

http://dx.doi.org/10.1016/j.ijfatigue.2017.08.009
0142-1123/

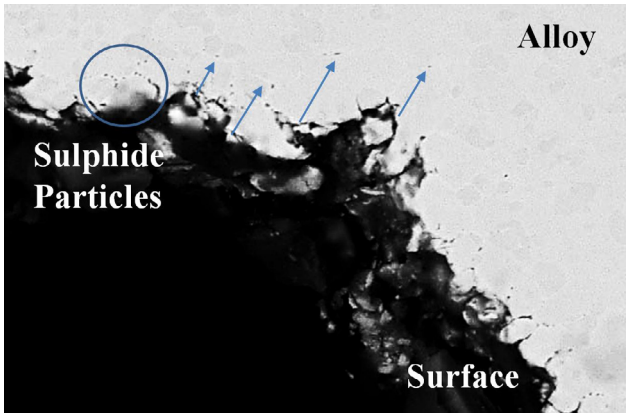

Fig. 1. Corrosion damage, displaying intergranular sulphide particles penetrating into the alloy from the surface (Courtesy of Rolls-Royce plc.).

at the melt/scale interface. The lack of oxide ions present in the deposit leads to solubility of the protective scale into the molten deposit as oxide ions are donated to the deposit by the protective oxides. Following dissolution and subsequent penetration of the protective scale, the molten deposit reaches the alloy surface and high sulphur activity in this region causes the precipitation of a continuous sulphide layer.

In components, sulphide particles may be seen at the grain boundaries ahead of corrosion features which demonstrates similarities to a transitional-type hot corrosion morphology [7] where at type-II temperatures, the sulphides of Cr and Ti appear as interconnecting sulphide networks at the grain boundaries. Earlier work suggests that the nucleation of grain boundary sulphides under type-II conditions arises from the decomposition of the melt such that it is no longer present at the metal surface as a continuous layer [8]. With the progress of time, this discontinuity renders the surface scale in contact with the ambient atmosphere allowing the introduction of sulphide particles to the grain boundaries from the sulphide layer via sulphidation-oxidation processes [8]. As shown in a hot corrosion assessment of RR1000 [1], the change in corrosion morphology from a continuous sulphide layer to grain boundary sulphide particles can be achieved under type-II conditions by significantly reducing the deposit flux.

Currently there is a lack of research considering the effect of transitional type hot corrosion on the remnant fatigue resistance of Ni-disc alloys. The majority of the published work addresses the impact of a classical type-II hot corrosion mechanism on fatigue life [9,10], where the methodology involves pre-pitting specimens prior to fatigue, a commonly used technique across numerous alloy systems. Whilst pre-pitting provides an ability to rank disc alloys based on their resistance to corrosive attack, subsequently fatigue testing pre-pitted specimens assumes that corrosion acts independently of stress. The resultant corrosion morphology achieved post-test displays thick oxide scales and evidence of pit coalescence leading to net section loss or broad front attack. In addition, the lack of diffused sulphur along the grain boundaries ahead of the advancing oxide front in areas of high stress concentration highlights the limitations of pre-pitting experiments in replicating service corrosion in the laboratory and suggests that the deposit flux is in excess of what is required to generate representative corrosion morphology. In this research, cylindrical round bar specimens are pre-notched to simulate the stress concentrating effect of the observed corrosion damage and subsequently corroded with a low flux of salt to simulate the transitional type hot corrosion morphology. The specimens are then subjected to a series of fatigue testing in an air environment to investigate the impact of representative corrosion features on cyclic life.

2. Experimental program

The pre-notched and corroding process the specimens undergo is described schematically in Fig. 2. Here, a micro-notch geometry is machined into the test specimen prior to low salt flux corrosion to precipitate grain boundary sulphide particles akin to stress assisted corrosion morphologies. Subsequent investigations into the effect of stress level on the low cycle fatigue response of corroded material can then be performed whilst considering the stress raising potential of the pit shaped notch features typically formed during corrosion-fatigue.

2.1. Material and specimens

The alloy used in this study is RR1000, a γ' precipitation-hardened Ni-based disc alloy developed by Rolls-Royce plc. for jet engine disc rotor applications. It has a nominal composition (in wt.%) of 18.5Co-15Cr-5Mo-3.6Ti-3Al-2Ta-0.5Hf-0.03C-0.02B-0.06Zr, balance Ni [11]. Material for this work was taken from forged and fully heat-treated material. A sub-γ' solvus heat treatment was used to generate a Fine Grain (FG) variant of RR1000 with a grain size between 5 and 10 μm.

Fatigue testing was performed using 11-off pre-notched (5-off of which were pre-corroded) FG RR1000 specimens which were compared to 15-off plain and un-corroded FG RR1000 specimens. The specimen design used was a cylindrical round bar of Ø4.5 mm and 12 mm gauge length. Prior to pre-notching and corrosion the specimen surfaces were machined to a specification of Ra < 0.25 μm and all specimens were subsequently shot peened at Metal Improvements Company (Derby, UK) to a specification of 6–8 Almen intensity and 200% coverage using 110H steel cast shot media.

2.2. Pre-notching and corroding

For the 11-off pre-notched specimens, three fully circumferential notches were machined to a depth of 40 μm, with a root radius of 50 μm into the gauge section. The machining process involved rotating the test specimen at 600 rpm perpendicularly against a fixed carbide cutting tool with the desired notch profile preformed on the tip. During turning, high pressure coolant was applied to eliminate the likelihood of brittle 'white layer' formation [12] commonly associated with rapid heating/quenching during the machining of Ni-alloys [13]. The notches were spaced 3 mm apart (see Fig. 3(a)) to ensure that each notch was a separate stress concentrating entity, i.e. when stress is applied; a nominal surface stress level is measured at the midpoint between two adjacent notches. Prior analysis via an axis-symmetric finite element (FE) model constructed during this research was used to verify that the design of the notches resulted in a constant stress concentration factor, $K_t = \sim 2.7$, and to verify that adjacent notch stress fields are independent. Fig. 3(a) illustrates the specimen design and Fig. 3(b) shows a digital microscope surface reconstruction of a selected notch from a machined specimen. This method allowed fatigue failure at one notch location, leaving the remaining intact notches for post-test mechanistic investigation. Prior to corrosion, the notched specimens were submerged in a neutral cleaning agent and placed in an ultrasonic bath to lightly remove loose machining debris and any residual coolant that may have remained.

Prior to fatigue testing, 5-off pre-notched specimens were salted using a micro-pipette technique, using a fully-saturated solution containing 98% Na_2SO_4 – 2% NaCl mixture dissolved in diluted methanol. These specimens were pre-heated to 100 °C on a hotplate and the solution was applied to the specimen gauge with a fine tip micro-pipette to allow access to the small notch features. The specimens were corroded under stress free conditions

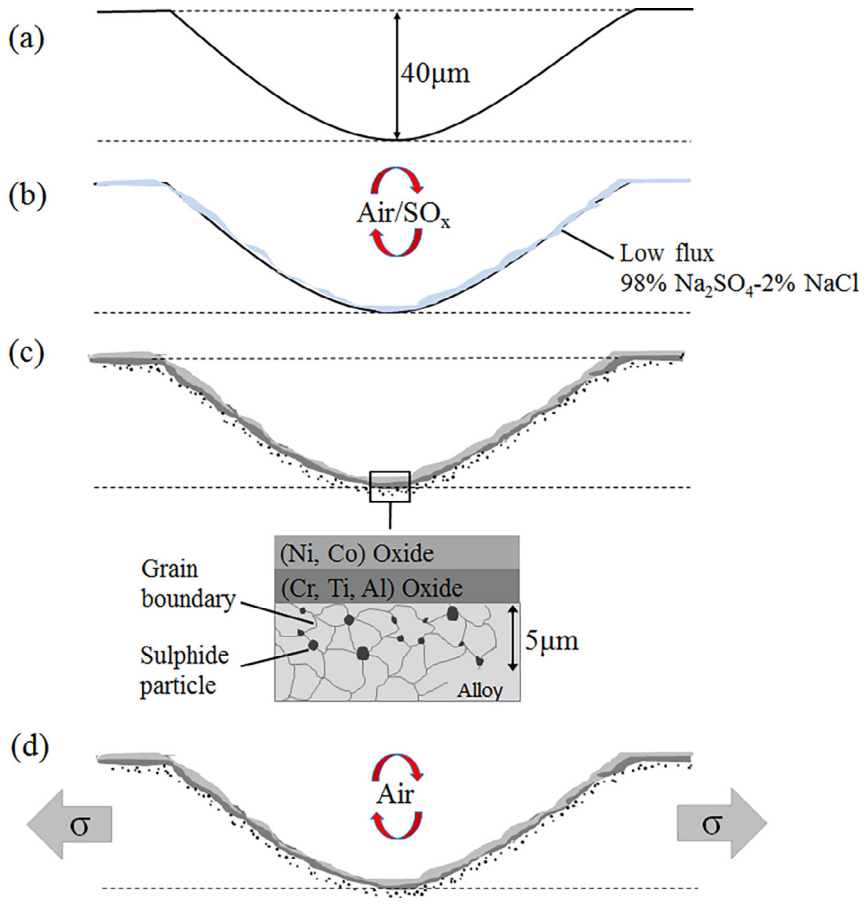

Fig. 2. Schematic diagram describing the experimental procedure for simulating corrosion damage and subsequent air fatigue testing (a) 40 μm Pre-notch, (b) hot corrosion under low flux conditions, (c) representative corrosion feature generated after 200 h showing the intergranular distribution of sulphide particles, (d) uniaxial fatigue test in air.

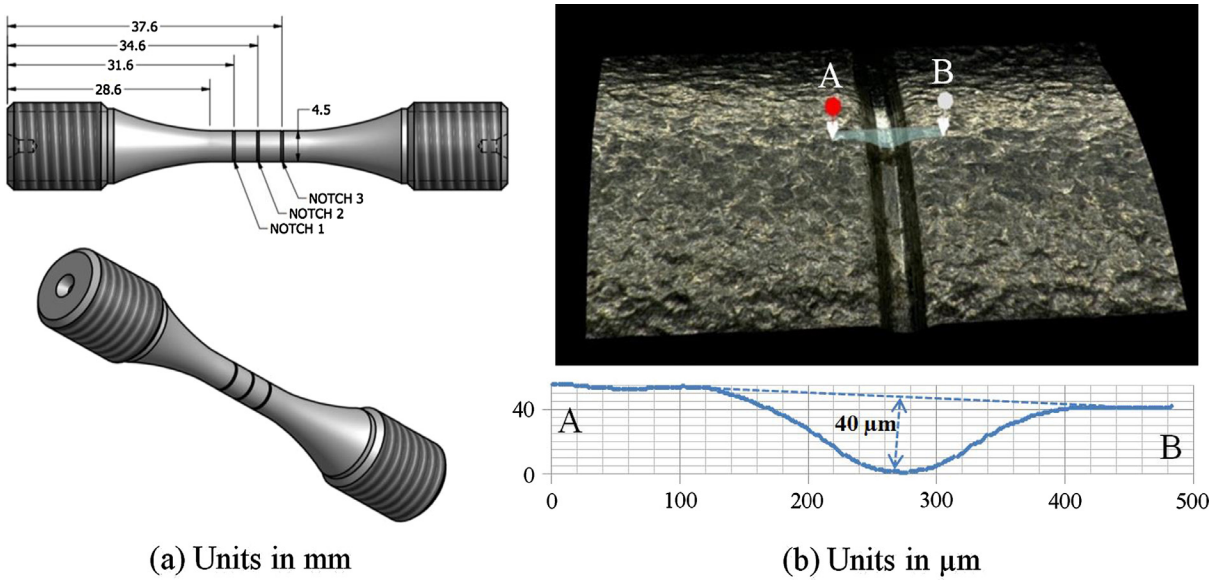

Fig. 3. (a) CAD reconstruction of the pre-notched specimen design used for testing and (b) a digital microscope reconstruction of a selected notch, verifying the measured notch depth of 40 μm.

in an air-300 ppm SO_2 environment at 700 °C for 200 h. A schematic diagram of the hot corrosion chamber used to conduct this experiment is presented in Fig. 4. Such conditions were designed to result in exhaustion of the salt deposit and the nucleation of representative corrosion features in the notch including both the surface scale and sub-surface sulphide penetration into the bulk.

2.3. Fatigue testing and analysis

All specimens were fatigue tested in an air-only environment at 700 °C. The applied stress range is designed to generate endurance lives between 15 and 150k cycles, using a fully reversed (R = −1) application of controlled load, over a six-second saw tooth waveform to limit the effects of creep and maximise time at temperature. The highest test stress was calculated based on the net cross section of the specimen taking into account the depth of the machine notch

Following fatigue testing, the specimens were sectioned, mounted and polished to reveal the cross-section of the notches through the primary initiation point along the specimen diameter. Examination of the cross-sections was performed mainly by Scanning Electron Microscopy (SEM) using a JEOL 35c microscope in secondary electron mode, with beam energy of 20 keV set to a working distance of ~10 mm. Chemical analysis was conducted by Energy-dispersive X-ray Spectroscopy (EDS) to characterise near surface composition and identify the potential abundance of specific elements, such as sulphur. For more detailed chemical analysis, Transmission Electron Microscopy (TEM) and EDS was carried out using a Tecnai T30 TEM in High-Angle Annular Dark Field (HAADF) imaging mode.

3. Results and discussion

Fig. 5 presents the S-N fatigue data of plain, pre-notched and pre-notched and corroded specimens.

The un-corroded pre-notched fatigue data shows an approximate 10% strength reduction when compared to plain specimens due to the stress concentrating effect of the notch, consistent across the range of tested stresses. Analysis of the pre-notched and corroded data shows that the results can be divided into two distinct regimes, a low stress regime ($\sigma_{norm} < \sim 0.73$), where a further 8% strength reduction is observed compared to the un-corroded pre-notched data and a high stress regime ($\sigma_{norm} = 0.79$) where a much larger strength reduction is observed. An explanation for these results can be derived from the cross-sectional analysis of the pre-notched and pre notched and corroded specimens.

3.1. Key observations

Prior to fatigue testing, the presence of sub-surface sulphide particles at the grain boundaries causes an alteration in the near surface alloy chemistry through the reaction of sulphur with Ti and Cr causing the local depletion of these elements and a weakened structure, shown in the EDS analysis in Fig. 6.

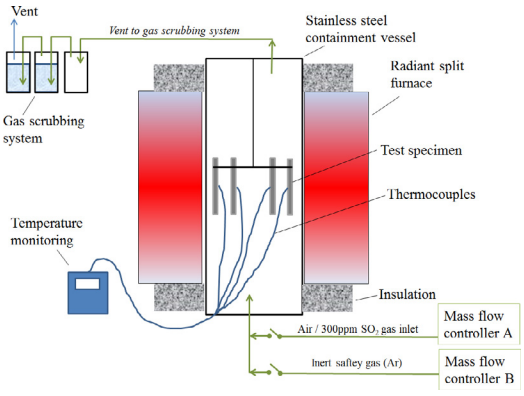

Fig. 4. Schematic illustration of the hot corrosion chamber used to corrode salt coated test specimens in an air-300 ppm SO_2 environment at 700 °C.

In general, enhanced fatigue crack initiation at elevated temperatures in an air environment has been shown to occur by cracking of the oxide scale [14]. More specifically, a corrosion-fatigue life comparison of a 12 wt%-Cr turbine blade steel demonstrated that the waveform most detrimental to life is not duration at peak stress as expected, but increased frequency of cyclic loading [15]. With this in mind it is possible that the alternating stress associated with the applied waveform resulted in continual surface oxide rupture, rendering the alloy unable to reform the protective scale, exposing the grain boundaries to further degradation. Fig. 7 suggests that during the fatigue cycle, rupture of the protective surface scale, which in this instance is dependent on the local stress magnitude (i.e. the notch root), exposes the sulphide containing bulk material to further oxidation. As the sulphides oxidise, the concentration gradient at the surface causes liberated sulphur in solid solution to diffuse down the grain boundaries to react with further Cr and Ti leading to the precipitation of fresh sulphides. Evidence of this self-sustaining mechanism is captured clearly in Fig. 7, where a comparison by metallographic assessment is made before (Fig. 7(a)) and after (Fig. 7(b)) the air fatigue testing of a pre-notched and corroded specimen at low stress. The progressive inward migration of sulphide particles as a result of their successive oxidation is shown to increase from the initial 5 μm depth to an effective depth of approximately 20 μm even in the absence of a corrosive environment. The effective depth in this case arises due to lateral diffusion of sulphur as a result of the oxidation of sulphides normal to the crack growth direction highlighted in Fig. 7 (b).

The most cited hot corrosion mechanism that leads to self-sustaining attack in an environment absent of gaseous SO_2 involves a reaction between the Na_2SO_4 deposit and refractory element additions, such as Molybdenum, added to superalloys for solid solution strengthening benefits. The mechanism, known as alloy-induced acidic fluxing, causes increased rates of corrosion due to high oxide ion activity in Na_2MoO_4 which leads to acidic fluxing of the protective scale [16]. In addition, the acidic component, MoO_3, can continually form at the alloy/Na_2SO_4 interface and evaporate at the Na_2SO_4/gas interface, maintaining key solubility criteria [4,17]. Given both the absence of SO_2 during fatigue and exhaustion of the salt deposit following the pre-corroding stage, a more applicable diffusion principle is discussed in an early sulphidation study on a Co-alloy [18]. Here, sulphur released by the oxidation of preformed sulphides was shown to diffuse into the alloy with no observed outward diffusion of sulphur and the self-sustaining nature of the mechanism was described to lead to increased deterioration of the alloy structure [19].

In fatigue, intergranular crack propagation in an air environment is frequently attributed to either grain boundary decohesion ahead of the crack tip as a result of dynamic embrittlement [20] or cracking at the grain boundary oxide/matrix-oxide interface as a result of stress assisted grain boundary oxidation [21]. An increasing number of studies [22,23] support the formation of oxides such as NiO, Cr_2O_3, TiO_2 and Al_2O_3 at the grain boundaries of Ni-disc alloys during crack propagation in preference to elemental oxygen penetration due to the free-energy change on their formation being more negative than possible grain boundary binding energies [24]. Moreover, metallographic inspection of RR1000 following long fatigue crack growth testing revealed that at a secondary crack tip, the layered oxide intrusion ahead of the propagating crack was intact ahead of a cracked oxide wake, which further verified that grain boundary oxidation occurs prior to grain boundary cracking [21,25]. In this study, as very thin grain boundary oxides are difficult to observe using SEM, a TEM foil of a near-surface region of disc alloy, corroded under conditions sufficient to produce sulphides at the grain boundaries was extracted and thinned using a Focused Ion Beam

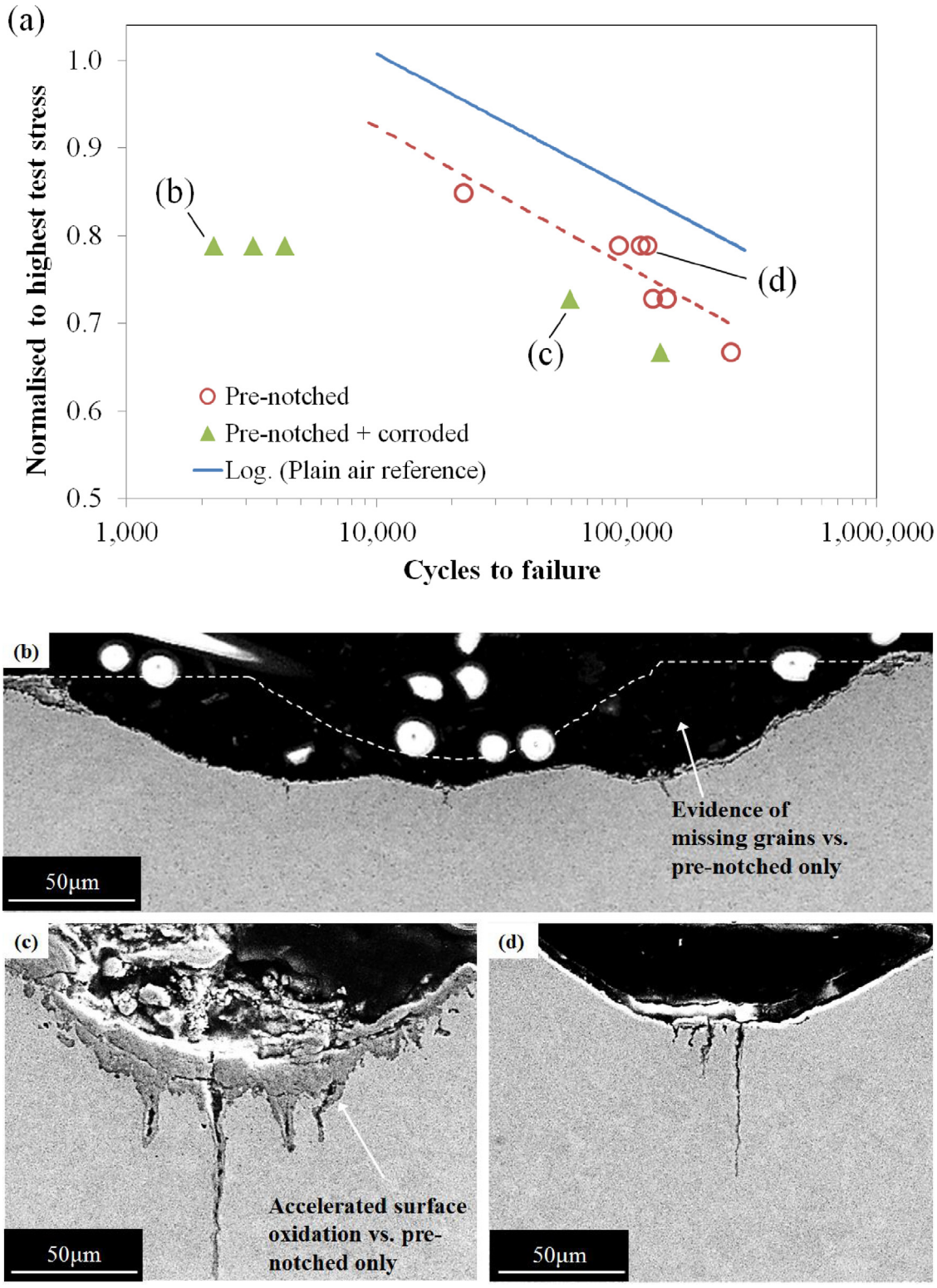

Fig. 5. (a) Cyclic endurance lives of pre-notched (circles) and pre-notched + corroded (triangles) RR1000 specimens compared to a plain RR1000 air reference line. Annotations correspond to SEM micrographs of notch cross sections at non-failure locations of specimens (b) pre-notched and corroded at $0.79\sigma_{norm}$ showing an outline of the original notch and evidence of missing grains, (c) pre-notched and corroded at $0.73\sigma_{norm}$, showing accelerated surface oxidation in comparison to air only (d) pre-notched at $0.79\sigma_{norm}$.

(FIB), the method of which is described in [26]. The resultant micrograph and EDS mapping from high resolution TEM analysis is shown in Fig. 8. Whilst the external Ni and Co scales have likely been removed during the preparation stage, the analysis demonstrates the presence of an internal grain boundary oxide mostly rich in Al and an external Cr Oxide approximately 5 μm thick. In addition, sulphide particles rich in Ti can be seen decorating the grain boundaries.

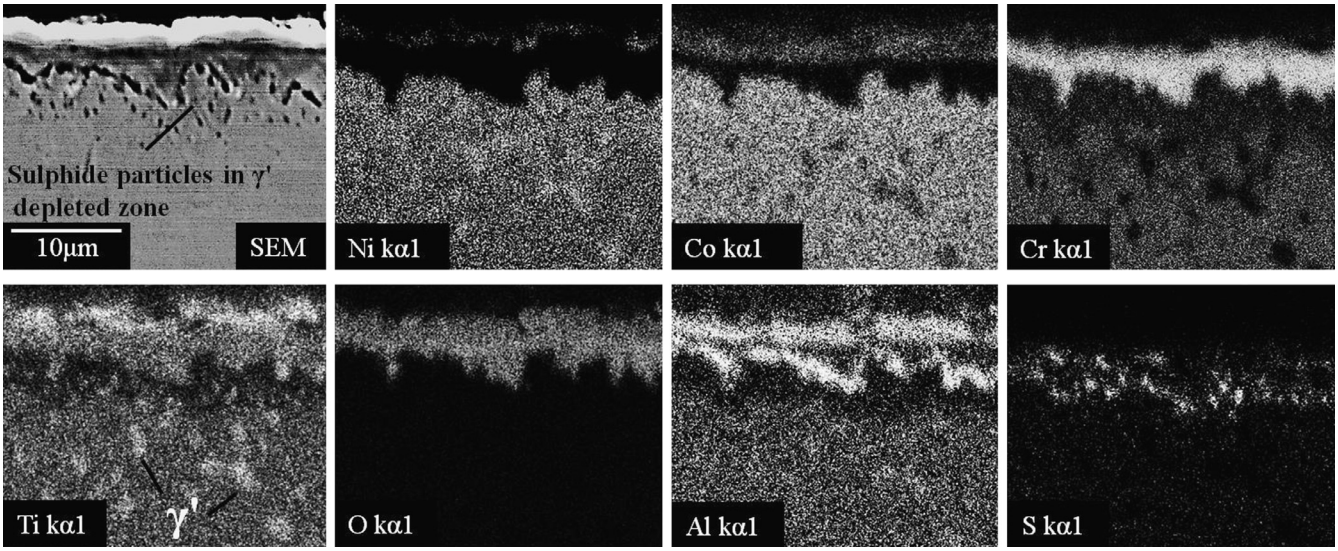

Fig. 6. SEM-EDS analysis at the surface of RR1000, corroded under low flux hot corrosion conditions, showing grain boundary sulphide particles and corresponding γ'-stabilising and scale forming element depletion.

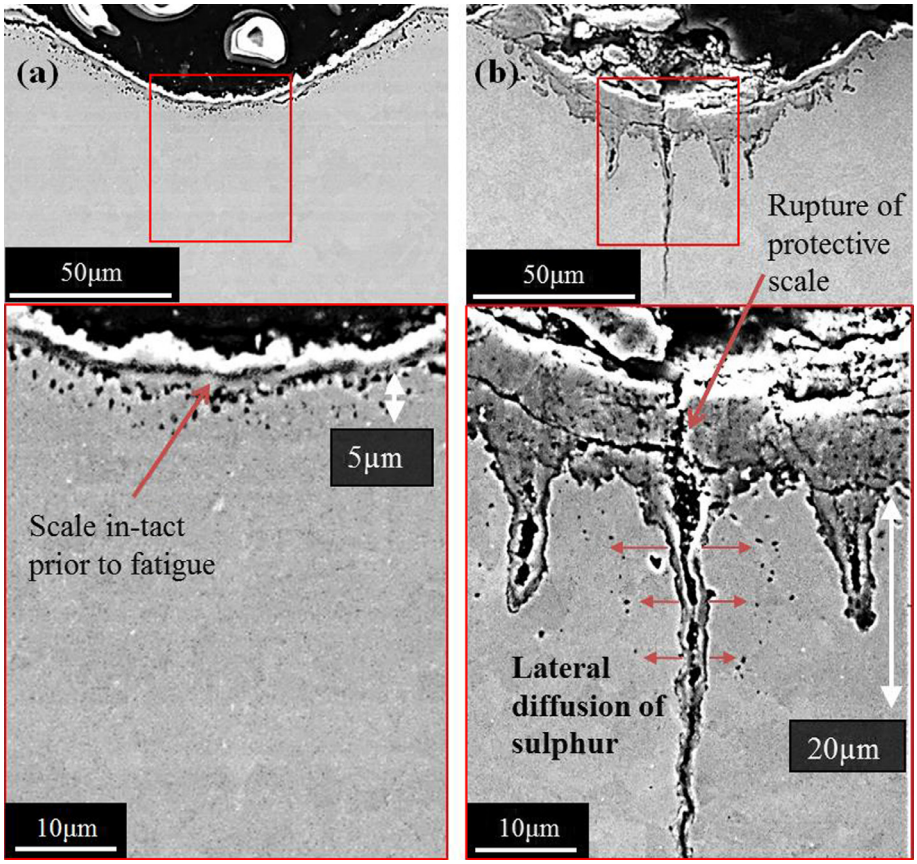

Fig. 7. SEM micrographs of notch cross sections of (a) pre-notched and corroded specimen before fatigue testing and (b) pre-notched and corroded specimens after fatigue testing at low stress showing a failure of the protective scale at a high local stress region and the inward migration of sulphide particles.

Whilst the composition of the oxides formed during this corrosion is consistent with those formed during the cyclic and isothermal oxidation of Ni-based alloys [27], typical post-air fatigue oxide thicknesses of RR1000 at 700 °C are comparatively low, ranging between 500 nm ± 140 nm [28]. These observations are in agreement with the evidence presented in Figs. 5 and 7, where accelerated surface oxidation is observed following the fatigue testing of corroded specimens in comparison to un-corroded specimens. The results suggest that the presence of sulphide particles at the grain boundaries is interacting with the oxidation process during fatigue and it is possible that the supply of oxide forming elements depleted in sulphide particle formation can provide an enhanced route to form a network of grain boundary oxide. On the basis of the present findings, a potential mechanism describing the effect

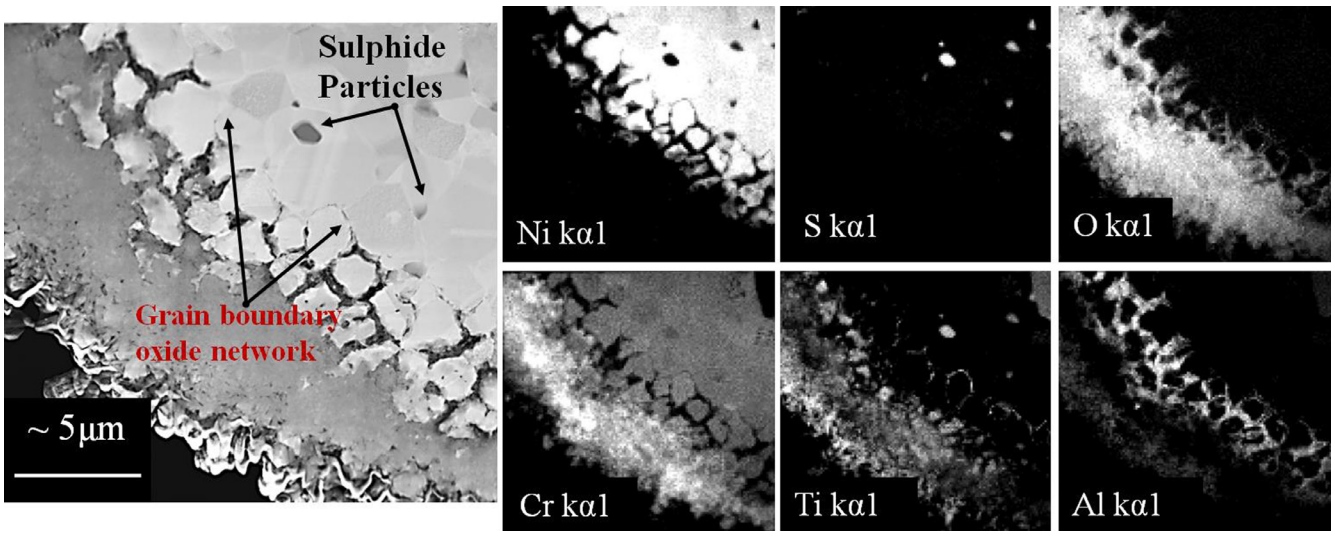

Fig. 8. TEM-EDS image of a disc alloy that was subject to hot corrosion, showing evidence of sulphide penetration ahead of a network of grain boundary oxide rich in Al.

of stress level on the enhanced failure of pre-notched and corroded specimens is discussed below.

3.2. Effect of stress level

The fracture surface of a pre-notched specimen tested at high stress shown in Fig. 9(a) displays multiple initiation sites and the maximum measured notch depths following failure were recorded at of 40 µm, shown schematically in Fig. 9(b). In comparison, the fracture surfaces shown in Fig. 9(c) and (e) for pre-notched and corroded specimens typically display a dominant initiation site at the deepest corrosion feature, measured at 49 µm and 78 µm for specimens tested at a low and high stress respectively. In addition, evidence of secondary sites exist around the perimeter; indicating that the corrosion is not isolated to a specific region within the notch. From fractography alone, the exact depth of the corrosion feature developed at low stress was difficult to distinguish due to the build up of oxidation product, however at high stress, a considerable amount of missing grains is observed, displayed schematically in Fig. 9(d) and 9(f).

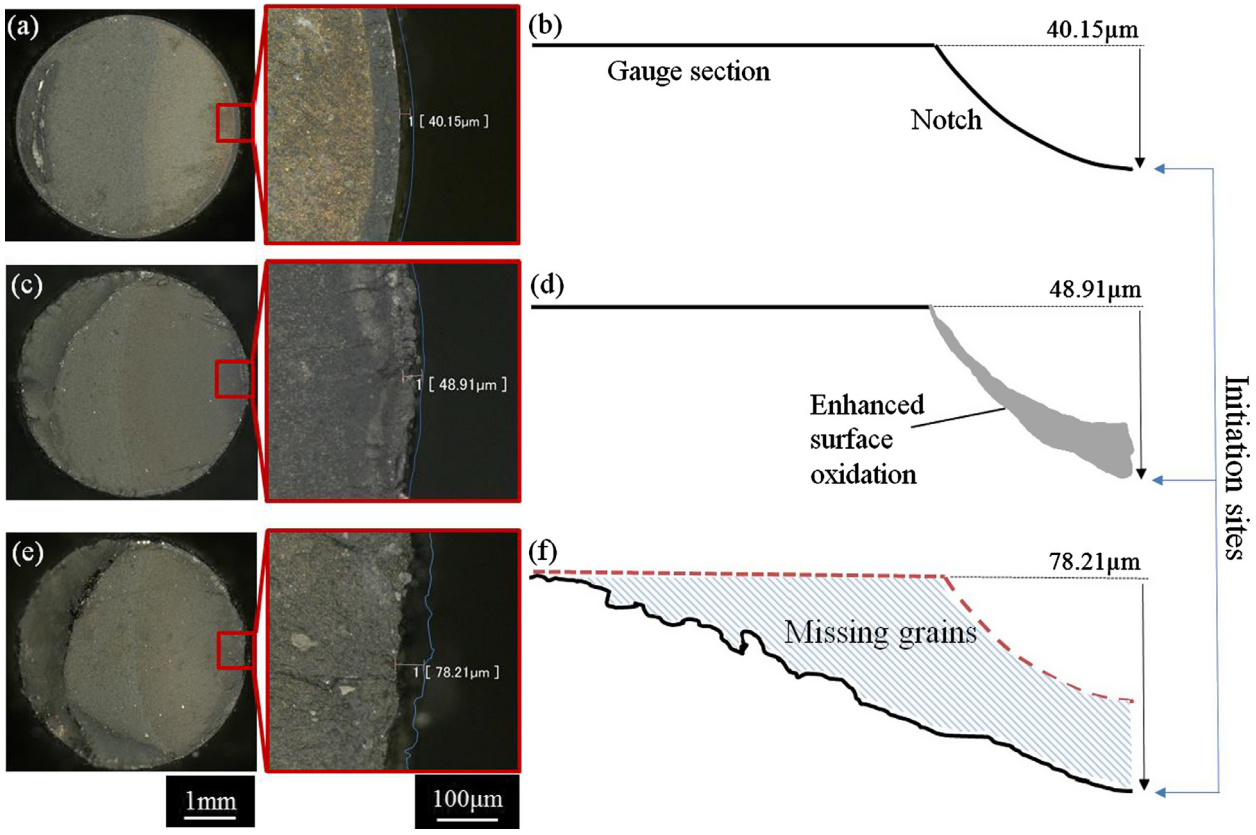

Fig. 9. Fracture surface and corresponding cross sectional schematic respectively of a (a), (b) pre-notched specimen fatigue tested at high stress (c), (d) pre-notched and corroded fatigue specimen tested at low stress and (e), (f) pre-notched and corroded fatigue specimen tested at high stress.

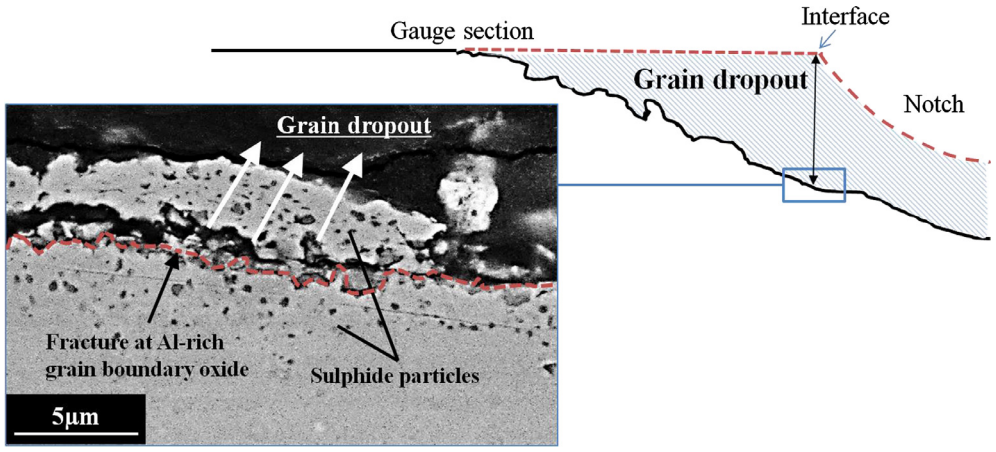

Fig. 10. Evidence of grain dropout in a pre-notched and corroded specimen fatigue tested at high stress, where the maximum depth of grain dropout occurred at the gauge/notch interface.

At temperatures above 750 °C, increasing the level of stress applied to RR1000 has been previously shown to accelerate oxidation processes, most predominantly at the grain boundaries where the high density of dislocations and vacancies is expected to enhance the diffusion of oxide forming elements [28,29]. If it is possible that grain boundary oxidation can be accelerated by increasing stress then it is reasonable to assume that in regions rich in sulphides, the rate of grain boundary sulphide particle oxidation will also increase. As demonstrated earlier, the oxidation of sulphides leads to the migration of sulphide particles deeper into the alloy, depleting oxide forming elements and further encouraging grain boundary oxidation.

Whilst this provides an explanation for the enhanced oxidation of corroded material in comparison to un-corroded material during fatigue, an explanation for the missing grains at high stress can be determined by considering the mechanical properties of a grain boundary oxide. A novel method to determine the fracture toughness of oxidised grain boundaries of a Ni-alloy was conducted by micromechanical testing of FIB machined cantilevers [30]. The results of the study showed that specimens containing oxidised grain boundaries fractured at the boundary following small amounts of plasticity, whereas specimens with un-oxidised boundaries yielded but did not fracture. In addition, a slight correlation existed between oxide thickness and fracture toughness value such that the grain boundaries became weaker with increasing oxide thickness [30]. In the present work, inspection by cross-sectional SEM analysis of a specimen tested in the high stress regime revealed the source of the missing grains, shown in Fig. 10, where multiple γ-grains with sulphide rich boundaries became detached from the bulk alloy leading to grain dropout. The mechanism demonstrates that when the stress level is sufficiently high, fracture through the grain boundary oxide proceeds, leading to grain dropout. This phenomenon is likely due to the expected mismatch in fracture toughness of the oxide with the Ni-alloy at elevated temperatures where values for Al_2O_3 and Ni-alloy are 3.6 MPa·$m^{\frac{1}{2}}$ [31] and 88 MPa·$m^{\frac{1}{2}}$ [32] respectively in the temperature range of 700–760 °C.

Comparable effects have been described in a study investigating hot corrosion behaviour on the LCF response of a Ni-base superalloy in an air environment [33]. The work showed that dissolution of the protective chromium oxide during hot corrosion leads to localised oxidation of the grain boundaries, providing multiple sites for crack initiation and growth. Similarly, a significant life reduction was observed as fatigue cracks initiated at the oxidised boundaries leading to what was described as catastrophic failure due to grain dropout [33]. Fig. 10 demonstrates schematically that largest depth of missing grains was found at the gauge-notch interface, a result which can be verified by observing the in-tact cross section shown in Fig. 5(c). Whilst more work is required to determine the precise sequence of sulphide migration and grain boundary oxide cracking, an initial explanation may be related to the stress field around the corrosion feature developed under loading. In general, pitting corrosion has been shown to have a detrimental effect on fatigue life and it is well documented that corrosion pits formed at the surface act to raise the stress locally. On loading, this may cause the corrosion pit to transition into a mechanical crack [34]. In contrast to what was expected, a stress corrosion cracking study conducted on Ni-Cr-Mo-V steel demonstrated that cracks formed from corrosion pits emanated from the mouth of the pit [35]. The research led to the development of an FE model [36], where it was shown that the maximum principle strain field was localised towards the pit-surface interface and it was determined that in order for the material to deform plastically, the material will yield where it is energetically most favourable, in regions of minimum constraint. Similar results were noted under more relevant environmental conditions, where fatigue testing of hot corrosion pitted Ni-disc alloy specimens displayed evidence of crack initiation along the grain boundaries connected to the pit surfaces [10]. Whilst these observations apply primarily to hemispherical pitting damage, irregularities of the post-fatigue fracture surface shown in Fig. 9(e) demonstrates that non-uniform metal wastage as a result of grain dropout may lead to localised regions of high strain, forcing grain boundary oxide cracking preferentially nearer to the notch-gauge interface. Regardless, the consecutive oxidation and fresh precipitation of sulphides deeper into the alloy is expected to propagate the proposed mechanism, leading to a level of grain dropout that leads to increased corrosion feature depth, contributing to the fatigue life reduction observed.

4. Conclusions

The fatigue test program conducted on pre-notched and pre-notched & corroded Ni-superalloy test pieces followed by extensive metallography; microscopy and image analysis has provided a detailed inspection of the evolution of corrosion damage during cyclic fatigue. As a result, a greater understanding of the response of corroded Ni-based superalloys in a fatigue environment has been obtained.

- Following 200 h of pre-exposure of a notch feature to an air-300 ppm SO_2 environment with a low deposit flux, the corrosion morphology exhibits intergranular subsurface sulphide particles beneath a dual outer scale that is analogous to damage typically instigated by the presence of stress.
- Subsequent mechanical loading at 700 °C causes local rupture of the surface oxide in high stress notch regions exposing the substrate to further oxidation and the exposed sulphide containing material is likely to possess reduced mechanical properties and corrosion resistance following γ'-stabilizing and scale forming element depletion.
- Analysis of the fatigue results demonstrates that a critical stress level appears to exist in pre-notched and corroded specimens, above which a change in mechanism occurs whereby the grain boundary oxide most likely nucleated in the wake of sulphide particles, fractures around segments of grains, leading to a metal loss that contributes to a reduction in fatigue properties.
- The inward migration of sulphide particles deeper into the bulk alloy following their successive oxidation during fatigue serves to propagate the damage mechanisms, even in absence of a corrosive environment.

Acknowledgments

This research was funded under the EPSRC Rolls-Royce Strategic Partnership in Structural Metallic Systems for Gas Turbines (grants EP/H500383/1 and EP/H022309/1). The provision of materials and supporting information from Rolls-Royce plc. is gratefully acknowledged. Mechanical tests were performed by MD at Swansea Materials Research and Testing Ltd. (SMaRT).

References

[1] Cockings HL, Perkins KM, Dowd M. Influence of environmental factors on the corrosion-fatigue response of a nickel-based superalloy. Mater Sci Technol 2017;33(9):1048–55.
[2] Child DJ, Meldrum J, Onuwarolu P. Corrosion-fatigue testing of Ni-based superalloy RR1000. Mater Sci Technol 2017;33(9):1040–7.
[3] Eliaz N, Shemesh G, Latanision RM. Hot corrosion in gas turbine components. Eng Fail Anal 2002;9(1):31–43.
[4] Rapp RA. Hot corrosion of materials: a fluxing mechanism? Corros Sci 2002;44:209–21.
[5] Pettit F. Hot corrosion of metals and alloys. Oxid Met 2011;76:1–21.
[6] Gheno T, Gleeson B. On the hot corrosion of nickel at 700 °C. Oxid Met 2015;84(5):567–84.
[7] Viswanathan R. Investigation of blade failures in combustion turbines. Eng Fail Anal 2001;8:493–511.
[8] Whittle DP, Misra AK. Effects of SO_2 and SO_3 on the Na_2SO_4 induced corrosion of nickel. Oxid Met 1984;22(1):1–32.
[9] Mahobia GS, Paulose N, Mannan SL, Sudhakar RG, Chattopadhyay K, Srinivas NCS. Effect of hot corrosion on low cycle fatigue behavior of superalloy IN718. Int J Fatigue 2014;59:272–81.
[10] Gabb TP, Telesman J, Hazel B, Mourer DP. The effects of hot corrosion pits on the fatigue resistance of a disk superalloy. J Mater Eng Perform 2009;19(1):77–89.
[11] Knowels D, Manning AJ, Small CJ. US patent: a nickel base superalloy. EP1193321 A1; 2002.
[12] Herbert CRJ, Axinte DA, Hardy MC, Brown PD. Investigation into the characteristics of white layers produced in a nickel-based superalloy from drilling operations. Proc Eng 2012:1–6.
[13] Wusatowska-Sarnek A, Dubiel B, Czyrska-Filemonowicz A, Bhowal P, Ben Salah N, Klemberg-Sapieha JE. Microstructural characterization of the white etching layer in nickel-based superalloy. Metall Mater Trans A 2011;42(12):3813–25.
[14] Connolley T, Reed PAS, Starink MJ. Short crack initiation and growth at 600dC in notched specimens of Inconel 718. Mater Sci Eng A 2003;340(1):139–54.
[15] Perkins KM, Bache MR. Corrosion fatigue of a 12% Cr low pressure turbine blade steel in simulated service environments. Int J Fatigue 2005;27:1499–508.
[16] Bornstein NS, DeCrescente M. The relationship between compounds of sodium and sulphur and sulphidation. Trans Metall Soc AIME 1969;245.
[17] Rapp RA, Goto KS. Hot corrosion of metals by molten salts. Electrochem Soc 1981;1(159).
[18] El-Dahshan ME, Stringer J, Whittle DP. Effect of presulfidation on the oxidation behaviour of co-based alloys. Part II. Presulfidation at sulfur partial pressures below the dissociation pressure of cobalt sulfide. Oxid Met 1974;8(4):221.
[19] El-Dahshan ME, Whittle DP, Stringer J. Effect of presulfidation on the oxidation behavior of co-based alloys. Part I. Presulfidation at sulfur partial pressure above the dissociation pressure of coblt sulfide. Oxid Met 1974;8(4):179.
[20] McMahon CJ, Pfaendtner JA. Oxygen-induced intergranular cracking of a Ni-base alloy at elevated temperatures – an example of dynamic embrittlement. Acta Mater 2001;49:3369–77.
[21] Kitaguchi HS, Li HY, Evans HE, Ding RG, Jones IP, Baxter G, et al. Oxidation ahead of a crack tip in an advanced Ni-based superalloy. Acta Mater 2013;61:1968–81.
[22] Molins R, Hochstetter G, Chassaigne JC, Andrieu E. Oxidation effects on the fatigue crack growth behaviour of alloy 718 at high temperature. Acta Mater 1997;45(2). 663–647.
[23] Miller CF, Simmons GW, Wei RP. Evidence for internal oxidation during oxygen enhanced crack growth in P/M Ni-based superalloys. Scr Mater 2003;48(1):103–8.
[24] Evans HE, Li HY, Bowen P. A mechanism for stress-aided grain boundary oxidation ahead of cracks. Scr Mater 2013;69:179–82.
[25] Jiang R, Everitt S, Lewandowski M, Gao N, Reed PAS. Grain size effects in a Ni-based turbine disc alloy in the time and cycle dependent crack growth regimes. Int J Fatigue 2014;62:217–27.
[26] Child DJ. Corrosion fatigue interactions of high temperature nickel alloys. Loughborough University Institutional Repository; 2012.
[27] Chen JH, Rogers PM, Little JA. Oxidation behavior of several chromia-forming commercial nickel-base superalloys. Oxid Met 1997;47(5/6):381–410.
[28] Foss BJ, Gray S, Hardy MC, Stekovic S, Mcphail DS, Shollock BA. Analysis of shot-peening and residual stress relaxation in the nickel-based superalloy RR1000. Acta Mater 2013;61(7):2548–59.
[29] Karabela A, Zhao LG, Tong J, Simms NJ, Nicholls JR, Hardy MC. Effects of cyclic stress and temperature on oxidation damage of a nickel-based superalloy. Mater Sci Eng A 2011;528(19–20):6194–202.
[30] Stratulat A, Roberts SG. Micromechanical testing of oxidised grain boundaries in Ni Alloy 600. Mater Res Soc 2013;1514:119–24.
[31] Sglavo VM, Trentini E, Boniecki M. Fracture toughness of high-purity alumina at room and elevated temperature. J Mater Sci Lett 1999;18:1127–30.
[32] Bahr DM, Johnson WS. Temperature dependent fracture toughness of a single crystal nickel superalloy. J ASTM Int 2005;2(4):346.
[33] Sahu JK, Gupta RK, Swaminathan J, Paulose N, Mannan SL. Influence of hot corrosion on low cycle fatigue behavior of nickel base superalloy SU 263. Int J Fatigue 2013;51:68–73.
[34] Chen GS, Liao CM, Wan KC, Gao M, Wei RP. Pitting corrosion and fatigue crack nucleation. Am Soc Test Mater 1997;1298:18–31.
[35] Turnbull A, Mccartney LN, Zhou S. Modelling of the evolution of stress corrosion cracks from corrosion pits. Corros Sci 2006;54:575–8.
[36] Turnbull A, Wright L, Crocker L. New insight into the pit-to-crack transition from finite element analysis of the stress and strain distribution around a corrosion pit. Corros Sci 2010;52(4):1492–8.